Journal of Electronics, Electromedical Engineering, and Medical Informatics
Multidisciplinary: Rapid Review: Open Access Journal **Vol. 7, No. 1, January 2025, pp: 208-219; eISSN: 2656-8632**

RESEARCH ARTICLE **OPEN ACCESS**

Manuscript received October 5, 2024; Revised December 1, 2024; Accepted December 12, 2024; date of publication January 30, 2025
Digital Object Identifier (**DOI**): https://doi.org/10.35882/jeeemi.v7i1.582

How to cite: Dwi Fitri Brianna, Lucky Indra Kesuma, Dite Geovani, and Puspa Sari, "Combination of Image Enhancement and Double U-Net Architecture for Liver Segmentation in CT-Scan Images", Journal of Electronics, Electromedical Engineering, and Medical Informatics, vol. 7, no. 1, pp. 208-219, January 2025.

Combination of Image Enhancement and Double U-Net Architecture for Liver Segmentation in CT-Scan Images

Dwi Fitri Brianna[1], Lucky Indra Kesuma[2], Dite Geovani[3], and Puspa Sari[4]

[1]Department of Informatics, Faculty of Computer Science, Universitas Sjakhyakirti, Palembang, 30145 Indonesia
[2]Department of Information System, Faculty of Computer Science, Universitas Sjakhyakirti, Palembang, 30145 Indonesia
[3]Department of Engineering, Faculty of Engineering, Universitas Sriwijaya, Palembang, 30128, Indonesia
[4]Department of Mathematics, Faculty of Mathematics and Science, Universitas Sriwijaya, Indralaya, 30862, Indonesia

Corresponding author: Dwi Fitri Brianna (e-mail: dwif.b933@ymail.com).

The authors would like to thank the Ministry of Education, Culture, Research, and Technology for supporting this research."

ABSTRACT Liver cancer can be identified using CT-Scan liver image segmentation. Liver segmentation can be performed using CNN architecture like U-Net. However, the segmentation results using U-Net architecture are affected by image quality. Low image quality can affect the accuracy of segmentation results. This study proposes a combination of image enhancement and segmentation stages on CT-Scan liver images. Image enhancement is achieved by using a combination of CLAHE to enhance contrast and Bilateral Filter to reduce noise. The segmentation architecture proposed in this study is Double U-Net which is a development of U-Net architecture by adding a second U-Net block with the same structure as a single U-Net. The first U-Net is used to extract simple features, while the second U-Net is used to extract more complex features and enhance the segmentation results of the first U-Net. PSNR and SSIM measure the results of image enhancement. The PSNR is more than 40dB and the SSIM result is close to 1. These results show that the proposed image enhancement method can enhance the quality of original images. The segmentation results were measured by calculating accuracy, sensitivity, specificity, dice score, and IoU. The result of liver segmentation obtained 99% for accuracy, 98% for sensitivity, 99% for specificity, 98% for dice score, and 90% for IoU. This shows that liver segmentation using Double U-Net obtained good segmentation. Results of image enhancement and image segmentation show that the proposed method is very good for enhancing image quality and performing liver segmentation accurately.

INDEX TERMS Image Enhancement, Segmentation, CLAHE, Bilateral Filter, Double U-Net.

I. INTRODUCTION

Liver cancer ranks sixth in the ranking of the most common cancers in humans. Liver cancer is caused by inflammation or cirrhosis of the liver [1]. Based on data from GLOBOCAN 2022, there were 866,136 cases of liver cancer with 758,725 deaths [2]. Liver cancer detection is performed by doctors and radiologists by manually observing CT-scan images of the liver. This observation is carried out to identify the tumor area and provide a mark by drawing a boundary line in the tumor area to obtain information in the form of volume, shape, and location of the tumor area [3]. This manual detection process is subjective, time-consuming, and susceptible to mistakes [4]. To overcome this, an automatic system is needed that can detect liver cancer more quickly and accurately, one of which is liver segmentation.

Liver segmentation is a technique used to separate liver from other organs in CT scan images. The results of liver segmentation can be used to diagnose liver diseases such as liver cancer [5]. Several studies on liver segmentation have been conducted using the watershed and adaptive threshold methods [6], morphological operators [7], and marker controlled watershed transform [8]. These studies still use

conventional methods, which are limited in handling large datasets, complex data features and variations, and data with overlapping features. One of the methods that can overcome the weaknesses of conventional methods is deep learning. A commonly used deep learning technique for segmentation is the Convolutional Neural Network (CNN) [9], [10]. CNN can extract and learn image features well so that it can produce good segmentation results [11], [12]. U-Net is a CNN architecture frequently employed for segmentation tasks [13]–[17]. U-Net is an architecture that effectively extracts image features. It consists of encoder, bridge, and decoder parts. The functions of the encoder part is to extract features, the decoder part functions to reconstruct features in the image, and the bridge functions to connect the encoder and decoder parts [18], [19]. Ozcan et al. [20] applied U-Net to liver segmentation produced a dice score of 87%, but IoU was still below 85%. Ayalew et al. [21] applied U-Net to liver segmentation resulted high accuracy above 95%. However, unfortunately, this study resulted dice score of below 75%. Liu et al. [22] implemented U-Net to liver segmentation, but dice score was still below 85%. The process of extracting image features in the encoder and reconstructing features in the decoder is influenced by image quality [23]. Low image quality can affect performance of segmentation results because it is prone to errors in extracting and reconstructing features [24], [25]. In liver segmentation, the quality of the CT-Scan liver image greatly affects the segmentation results. The quality of CT-scan images is affected by various factors, one of which is the technique used for image acquisition.

CT scan images are taken from a CT machine that emits X-rays [26]. X-rays are emitted using a low-dose technique that produces CT scan images that have low contrast accompanied by increased noise [22], [27], [28]. Low image quality can affect the accuracy of segmentation results because the model is prone to errors in learning and extracting features in the image [29]. To overcome this, a technique is needed to enhance contrast, one of which is Contrast Limited Adaptive Histogram Equalization (CLAHE) [30], [31]. CLAHE enhances contrast based on the distribution of pixel histograms in a certain area [32]. CLAHE can enhance image quality and help the model learn features in the image [33]. The quality of the enhanced image can be measured using various performance measures, including PSNR and SSIM [34], [35]. PSNR is used to measure the similarity between the original image and the enhanced image based on the amount of noise that has been successfully handled. The higher the PSNR result, the more noise has been removed. Good image quality has a PSNR above 30 dB [34], [36], [37]. SSIM is a measure of similarity that includes structure, brightness, and contrast between two images [38], [39]. The SSIM scale is between 0 and 1, the closer the SSIM value is to 1, the more similar the original image and the preprocessed image [38]. Umilizah et al. [40] applied contrast enhancement with CLAHE to CT SCAN liver images resulted SSIM of 0.7088. Siddiqi et al [31] applied contrast enhancement with CLAHE to CT-SCAN liver images resulted in average PSNR of 22.7 dB. In addition to low contrast, CT-scan image quality also has a high level of noise intensity. Noise in the image can make it difficult for the model to recognize features in the image, resulting in a decrease in the accuracy of the segmentation results [27]. One technique that can be used to reduce noise intensity in CT-scan images is a bilateral filter [41], [42]. Bilateral filter is an image processing technique used to smooth images by considering the distance and intensity between pixels [41]. The bilateral filter can reduce noise while maintaining the sharpness of the boundaries of each feature in the image [43]. Nguyen et al. [44] applied bilateral filter to CT-scan liver segmentation using U-Net architecture resulted a high dice score of above 95%. However, this study did not measure the performance evaluation of image quality enhancement such as PSNR and SSIM. Muthuswamy [45] applied the bilateral filter to CT-scan liver images resulted in a good PSNR of 35.11. Unfortunately, the result of SSIM was still low at 0.53.

In addition to being influenced by image quality, U-Net has shallow structure makes this architecture less capable of effectively extracting small features, especially in more complex liver tumor cases. Therefore, a new approach is needed to optimize segmentation performance. One such approach is the Double U-Net architecture, which leverages two integrated U-Net models to improve the extraction and reconstruction of detailed features, enabling more accurate and refined segmentation results compared to the standard U-Net [46], [47]. The first U-Net in the Double U-Net architecture is tasked with extracting simple features in images and performing initial segmentation. The second U-Net is tasked with improving the results of the first U-Net by learning more complex features and obtaining additional feature details and improving the model's ability to perform more detailed and accurate segmentation [48]–[50]. Double U-Net has not been applied to liver segmentation but has been applied to other segmentations. Jha et al. [47] applied Double U-Net to polyp, skin lesion, and nucleus segmentation resulting in more optimal segmentation than single U-Net.

This study aims to improve the quality of liver segmentation results on CT-scan images by overcoming the challenges caused by low image quality and the limitations of the U-Net architecture in extracting small features. To achieve this, this study proposed combines image quality enhancement and segmentation stage. In the image enhancement stage, a combination of CLAHE and bilateral filters is proposed. CLAHE enhances contrast in CT-scan images, improving visibility in low-contrast areas. Bilateral filters reduce noise while preserving edge sharpness. This combination improves CT-scan liver image quality, aiding segmentation models in feature extraction. In the segmentation stage, this study proposes Double U-Net architecture to achieve more optimal segmentation results. The first U-Net is responsible for extracting simple features from the liver image and performing initial segmentation. The second U-Net to refines these initial results by learning more complex features. The proposed method will classify the liver into two classes: liver and background. The success of the image enhancement stage

will be evaluated using PSNR and SSIM. PSNR is used to measure the comparison of emphasized noise, while SSIM is used to evaluate the structural similarity between the enhanced image and the original image. The success of the Double U-Net segmentation method is measured using metrics such as accuracy, sensitivity, specificity, dice score, and IoU to assess the precision and consistency of the liver segmentation results. Improved segmentation helps identify tumor boundaries, crucial for disease staging and treatment planning. It supports informed decisions, enhances patient care, and speeds up image analysis. The contributions of this study are as follows.

1. Model for image enhancement and segmentation of liver images.
2. Liver segmentation performance is improved by a combination of CLAHE and bilateral filter methods with Double U-Net architecture.
3. The performance of the proposed model is measured by calculating the PSNR, SSIM, accuracy, sensitivity, specificity, dice score, and IoU.

II. METHODS

A. DATASET

The dataset used in this study is secondary data of liver CT scan images which can be accessed on the Kaggle website at https://www.kaggle.com/datasets/stevenazy/liver-dataset/data [51]. In this dataset, 800 images are consisting of 400 original images and 400 ground truth. The images in this dataset have a size of 256×256 pixels in Portable Network Graphics (*.png) format. Example of the display of original images and ground truth in this study can be seen in FIGURE 1.

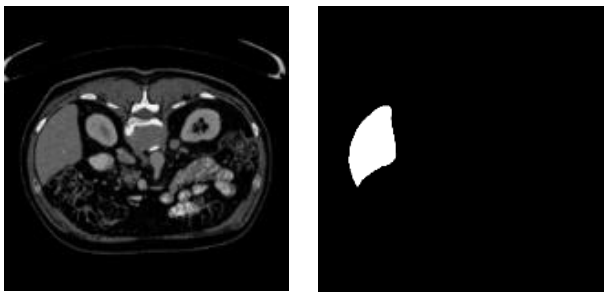

FIGURE 1. Example Displays of (a) Original Image (b) Ground Truth on Liver Dataset in This Study

B. PREPROCESSING AND IMAGE ENHANCEMENT

1. RESIZE

Resize is an adaptive change in image size without changing or removing important information contained in the image [19], [52], [53]. Resize aims to give the image have a more optimal appearance, the data used is not too large and is by the model to be used [19]. In this study, image resizing was carried out on all images to a size of 256×256 pixels.

2. AUGMENTATION

Augmentation is a process of increasing the amount of data by varying the data [54]–[57]. Augmentation enhances the model's capabilities to overcome limited data in research [58]–[61]. In this study, augmentation was carried out to increase the quantity of data, thereby improving the performance of the proposed model. In this study, the augmentation used is flipping. The flipping technique is horizontally, vertically, and horizontal-vertical. The flipping technique is used because it can produce new data by flipping images, thereby increasing the amount and variety of data without altering the image's features [62]. Examples of the results of image augmentation with augmentation with the flipping technique horizontally, vertically, and horizontal-vertical can be seen in FIGURE 2.

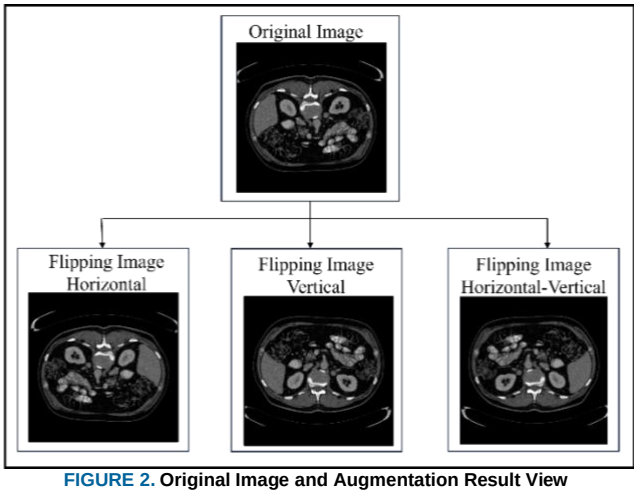

FIGURE 2. Original Image and Augmentation Result View

FIGURE 2 shows an example of the original image and the augmented image using horizontal, vertical, and horizontal-vertical flipping techniques to obtain a new image.

3. RGB

The image received from the input data is still in BGR (Blue Green Red) form. The image is converted from BGR (Blue Green Red) to RGB (Red Green Blue) which aims to make the image display more accurate [19].

4. GREEN CHANNEL

After the BGR image is converted to RBG, channel separation is performed on the image to take the green channel of the liver image. The separation of the green channel is done because the green channel in the liver image has a clearer appearance than the red and blue channels.

5. GRAYSCALE

In the grayscale stage, the green channel image is changed into a grayscale image. Grayscale has a color gradation range between black and white which is very suitable for image processing [63]. Changing the image to grayscale is done to clarify the contrast variations in the image [64]. The grayscale process is defined in Eq. (1) [64].

$$l_{i,j} = (r_{i,j} * 0.229) + (g_{i,j} * 0.587) + (b_{i,j} * 0.114) \quad (1)$$

where $l_{i,j}$ is the grayscale value with a range of 1-256 in the i-th row and j-th column, $r_{i,j}$, $g_{i,j}$, $b_{i,j}$ are the red, green, and blue channel value in the i-th row and j-th column.

6. CLAHE

The CLAHE method is used to display hidden features in an image by equalizing the histogram for each image pixel value. CLAHE works by providing a maximum limit value

for the height of a histogram (clip limit). Clip limit is used to divide the image into several small parts with identical sizes so that the histogram of the output image matches the histogram indicated by the distribution parameters [65]. The clip limit calculation process uses Eq. (2) [63].

$$c_{i,j} = \frac{k}{h}\left(1 + \frac{\alpha}{100}(l_{max} - 1)\right) \quad (2)$$

where l_{max} is the maximum pixel value of the grayscale result pixel, $c_{i,j}$ is the clip limit value in the i-th row and j-th column, k is the area size, h is the grayscale value with a range of 1-256, and α is the clip factor with a range of 0-100

7. BILATERAL FILTER

Bilateral filter is one of the denoising techniques used to smooth images by considering the distance and intensity between pixels [41]. The bilateral filter can remove noise in the image and be able to maintain the image edge details effectively. In bilateral filter, each pixel in the image is replaced by the weighted sum of the pixel intensities nearby to remove noise. The weights of adjacent pixels are selected based on the Gaussian distribution [66]–[68]. The bilateral filter process can be seen mathematically in Eq. (3) [66].

$$B(x,y) = \frac{\Sigma x' \Sigma y' I(x',y') exp\left(-\frac{(x^2+y^2)}{2\sigma_s^2}\right)(x-x',y-y') exp\left(\frac{a^2}{2\sigma_r^2}\right)(I(x,y)-I(x'-y'))}{\Sigma x' \Sigma y' xp\left(-\frac{(x^2+y^2)}{2\sigma_s^2}\right)(x-x',y-y') exp\left(\frac{a^2}{2\sigma_r^2}\right)(I(x,y)-I(x'-y'))} \quad (3)$$

where $B(x,y)$ is the bilateral filter result at pixel point (x,y), (x',y') is the neighboring pixel of (x,y), (x,y) is the coordinates of the image pixel in the x-th row and y-th column, σ_s is the spatial kernel area, and σ_r is the minimum amplitude value.

C. DOUBLE U-NET ARCHITECTURE

Double U-Net architecture is a modification of the U-Net architecture. The Double U-Net architecture comprises two integrated U-Net models that enhance feature extraction and reconstruction, yielding more accurate and refined segmentation outcomes than the standard U-Net. Double U-Net architecture consists of two U-Net architectures combined into one unit in one training process. Double U-Net architecture implements the encoder and decoder processes in the first U-Net block. The output from the decoder stage in the first U-Net block is used as input to the encoder and decoder stages in the second U-Net block. The structure of the Double U-Net architecture can be seen in FIGURE 3.

FIGURE 3 shows the Double U-Net architecture consisting of two U-Net blocks, where each U-Net block consists of an encoder, bridge, and decoder path. The encoder section is used to convert the input image into a desired feature representation. The encoder section consists of 4 blocks, where each block consists of a 3×3 convolution process, ReLU activation function, batch normalization, and max pooling. The bridge section consists of a 3×3 convolution process, ReLU activation function, and batch normalization. The bridge section functions to connect the encoder section to the decoder.

The decoder section is used to map the obtained features. In the decoder section, there are 4 blocks consisting of upsampling, concatenate, 3×3 convolution, ReLU activation function, and batch normalization. The last block in the decoder section contains a convolution process with a filter size of 1 and a sigmoid activation function. The sigmoid activation function is used to get the output of the segmentation process. The output results obtained in the first U-Net block are used as input to the second U-Net block. The structure of the second U-Net block is the same as the structure of the first U-Net block. The output result of the second block of U-Net is the result of segmentation using the Double U-Net architecture.

The convolution operation is used to learn feature representations from the input. This layer consists of a set of convolutional kernels to extract local features from the inputs [69]. The calculation process of the convolution operation on the convolutional layer uses Eq. (4) [70]. This calculation are performed to build more complex features representation.

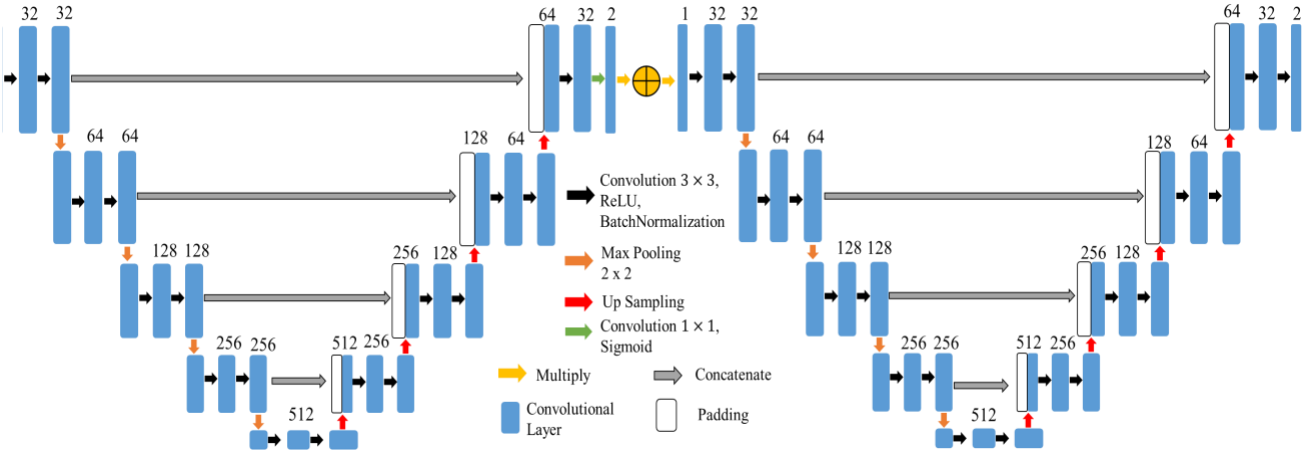

FIGURE 3. Double U-Net Architecture

$$v_{i,j} = \left(\sum_{u=0}^{n-1}\sum_{v=0}^{n-1} b_{u+i,v+j} \times k_{u+1,v+1}\right) + a_q \quad (4)$$

for $i = 1,2,\ldots,n$ and $j = 1,2,\ldots,n$, where $v_{i,j}$ is the entry of the convolution result matrix in the i-th row, j-th column,

$b_{u+i,v+j}$ is the entry of the input matrix in the $u+i$-th row, $v+j$-th column, $k_{u+1,v+1}$ is the entry of the kernel matrix in the $u+1$-th row, $v+1$-th column, and a_q is the bias for the q-th kernel. Rectified Linear Unit (ReLU) is one of the activation functions used in CNN where if the activation function input is negative, the output changes to zero [70]. Mathematically, ReLU can be defined in Eq. (5) [70]. The ReLU activation function is a non-linear function used in the model so that the network is able to learn complex feature patterns.

$$t_{i,j} = r(v_{i,j}) = \max(0, v_{i,j}) = \begin{cases} v_{i,j} & where\ \ v_{i,j} \geq 0 \\ 0 & where\ v_{i,j} < 0 \end{cases} \quad (5)$$

where $t_{i,j}$ is the output result of the ReLu activation function and $v_{i,j}$ is the input pixel value of the convolution operation result. The result of the ReLU activation function is normalized using batch normalization. Batch normalization can accelerate convergence, reduce dependence on weight initialization, prevent overfitting and improve generalization. Batch normalization is important to use in deep and complex models. Batch Normalization is a normalization process for each layer in the network that is applied before or after the activation function [71]. The calculation of the Batch Normalization result is done by first calculating the average (μ_j) and variance (σ_j^2), then normalizing it. The calculation process of the average (μ_j), variance (σ_j^2), and normalization is done using Eq. (6), (7), and (8) [70].

$$\mu_j = \frac{1}{m}\sum_{i=1}^{m} t_{i,j} \quad (6)$$

$$\sigma_j^2 = \frac{1}{m}\sum_{i=1}^{m}(t_{i,j} - \mu_j)^2 \quad (7)$$

$$g = \hat{t}_{ij} = \frac{t_{ij}-\mu_j}{\sqrt{\sigma_j^2+\varepsilon}} \quad (8)$$

where μ_j is the average value of each mini-batch, σ_j^2 is the variance value for each mini-batch, j is the number of mini-batches, m is the amount of data in a mini-batch, $\hat{t}_{ij}$ is the normalization result of the input value in the i-th row and j-th column, t_{ij} is the input matrix entry result from the ReLU activation function operation in the i-th row and j-th column, and ε is the smallest constant value.

The next operation is to reduce the dimensionality of the feature map resulting from batch normalization using maxpooling. Maxpooling works by dividing the input matrix into small sub-matrices and then taking the maximum value from each sub-matrix to produce a new matrix. In the decoder section, the same convolution layer, ReLu activation function, and batch normalization operations are performed as in the encoder section. In the decoder section, the dimensionality of the feature map is increased using upsampling. The results of the operations in the encoder and decoder sections are combined using concatenate. At the end of the decoder section, there is a sigmoid activation function calculation operation using Eq. (9) [72].

$$s = f(g) = \frac{1}{1+e^{-g}} \quad (9)$$

where s is the output of the sigmoid activation function and g is the input result of batch normalization. The last stage is the calculation of the loss function using binary cross entropy. Binary cross-entropy is a loss function used to calculate the loss in the case of two classes [73], [74]. Binary cross-entropy is calculated using Eq. (10) [75].

$$H_p(s) = -\frac{1}{n}\sum_{i=1}^{n}(s_i \times log\,(p(s_i) + (1-s_i) \times log(1-p(s_i)) \quad (10)$$

where n is the row of the prediction result matrix, s_i is the class in the classification, $p(s_i)$ is the probability value of s_i, and $H_p(s)$ is the binary cross entropy result value.

D. Evaluation Metrics

The success of the proposed method in this study was measured by calculating the performance evaluation. The success rate of image enhancement was measured by calculating the Peak Signal-to-Noise Ratio (PSNR) and Structural Similarity Index Measure (SSIM) values. PSNR is a metric that evaluates the effectiveness of noise reduction by measuring the peak signal-to-noise ratio. SSIM focuses on assessing the structural similarity between the processed image and the original, accounting for visual quality aspects such as luminance, contrast, and structure.

Accuracy represents the proportion of correctly predicted pixels. Sensitivity indicates the model's capability to identify the liver region within an image, and specificity measures the ability to differentiate background pixels. The Dice score quantifies the agreement between the segmented image and the ground truth, while IoU (Intersection over Union) evaluates the degree of overlap between the segmented image and the ground truth. The success rate of the Double U-Net architecture for performing liver segmentation on liver CT-Scan images was measured by calculating the accuracy, sensitivity, specificity, dice score, and Intersection over Union (IoU) values. The accuracy, sensitivity, specificity, dice score, and IoU score values were calculated using Eq. (11), (12), (13), (14), and (15) [76]–[80].

$$Acc = \frac{TP+TN}{TP+FN+FP+TN} \quad (11)$$

$$Sen = \frac{TP}{TP+FN} \quad (12)$$

$$Spe = \frac{TN}{TN+FP} \quad (13)$$

$$Dc = \frac{2TP}{2TP+FP+FN} \quad (14)$$

$$IoU = \frac{TP}{TP+FP+FN} \quad (15)$$

where TP is the proportion of positive cases predicted as positive cases, TN is the proportion of negative cases predicted as negative cases, FP is the proportion of negative cases predicted as positive cases, and FN is the proportion of positive cases predicted as negative cases [81]. These values are obtained at the testing stage. The performance evaluation results in this study will be compared with several previous studies to provide a comprehensive analysis and become a benchmark for the proposed approach. An illustration of the overall methods used in this study can be seen in FIGURE 4.

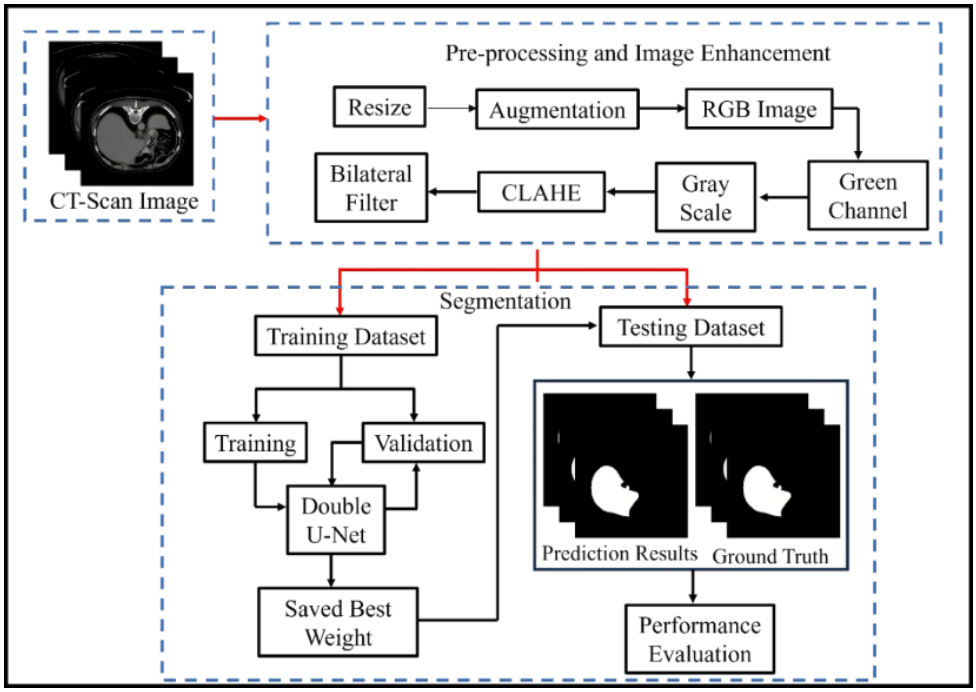

FIGURE 4. Overall, Method in Liver Segmentation on CT-Scan Images Using Double U-Net Architecture

III. RESULT AND DISCUSSION

A. PREPROCESSING AND IMAGE ENHANCEMENT

In the initial stage, the CT-scan image size was changed to 256 × 256 pixels. In the second stage, augmentation was performed using horizontal, vertical, and horizontal-vertical flipping techniques to increase the amount of image data. The augmentation stage produced 1,200 images so the latest amount of data was 1,600 images. 1,600 images consist of 400 original images, 400 horizontally flipped images, 400 vertically flipped images, and 400 images flipped both horizontally and vertically. The results of CT-scan augmentation with the BGR channel display were changed to RGB channels. In the RGB image, the green channel was separated for use in this study. Then, the green channel image was transformed into grayscale. After the image was converted to grayscale, CLAHE was applied to display hidden features in the image by equalizing the histogram for each image pixel value. In the final stage, a bilateral filter was implemented on the CLAHE image to reduce the intensity of noise in the image. An example of the display of the results of all the pre-processing and image enhancement stages carried out in this study can be seen in FIGURE 5.

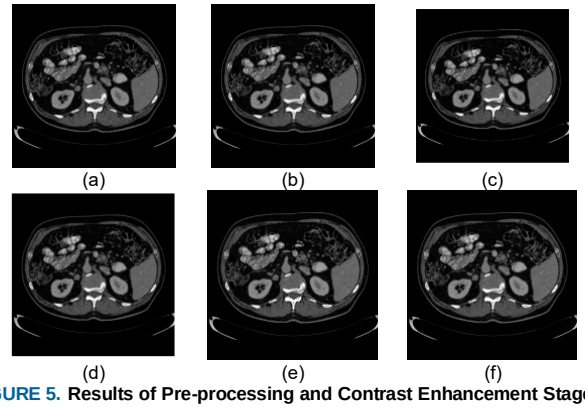

FIGURE 5. Results of Pre-processing and Contrast Enhancement Stage of CT-Scan Images (a) Augmentation (b) RGB Image (c) Green Channel (d) Grayscale (e) CLAHE (f) Bilateral Filter

Image enhancement produces an image that has been enhanced in quality from the original image, but the enhanced image still contains the same objects as the original image. Image enhancement does not produce a new image that is different from the original image, but produces the same image. The performance evaluation of the stages of improving the quality of CT-scan liver images from image enhancement is measured by calculating the PSNR and SSIM values which can be seen in TABLE 1.

TABLE 1
PSNR and SSIM Value of CT-Scan Image Enhancement Results

No	File Name	PSNR	SSIM
1	0000.png	40.33947	0.92627
2	0001.png	40.33466	0.92626
3	0002.png	40.33851	0.92626
.	.	.	.
.	.	.	.
.	.	.	.
1599	1598.png	41.40521	0.89753
1600	1599.png	41.41692	0.89753
Average		40.30562	0.92497

In TABLE 1, the average PSNR and SSIM values obtained have an average of 40.30562dB and 0.92497, respectively.

The image enhancement achieves a PSNR above 40dB, indicating high quality with minimal noise. The SSIM of 0.92497 shows the enhanced image closely resembles the original in structure, as perceived by human vision. Based on the results of the preprocessing and image enhancement stages, it can be concluded that the image from the image enhancement has good quality to be used as input at the segmentation stage.

B. SEGMENTATION WITH DOUBLE U-NET ARCHITECTURE

In the segmentation stage, the dataset is divided into two groups consisting of 80% training data, namely 1,280 images, and 20% testing data, namely 320 images. The training data is divided into two groups consisting of 80% training data, namely 1,024 images, and 20% validation data, namely 256 images. The parameters in the training process include epochs of 100, batch size of 5, and learning rate of 0.00001. The best weight value in the training process will be saved for use in the testing stage. During the training process, accuracy and loss values are measured to evaluate's model performance. The accuracy value is used to measure the success of the Double U-Net architecture in extracting liver features from CT-Scan images while the loss is measured to see the error rate in the Double U-Net architecture in recognizing liver features from CT-Scan images. The graph of accuracy and loss values obtained in the training process can be seen in FIGURE 6. During training, sensitivity and specificity are measured alongside accuracy and loss. Sensitivity indicates the model's ability to correctly identify relevant image features, while specificity measures its effectiveness in distinguishing accurate predictions from all predicted features. The graph of sensitivity and specificity values in the training process can be seen in FIGURE 7.

FIGURE 6(a) shows that the accuracy value in the training process is above 98%. Training and validation data accuracy increases steadily, stabilizing around the 40th epoch. A slight drop occurs at the 78th epoch, however the performances recovers and stabilizes again by the 80th epoch. FIGURE 6(b) shows that the loss value in the training process for the training data and validation data continues to decrease towards a value below 0.05. In the 78th epoch, the loss value on the training data and validation data increases slightly, but decreases again and stabilizes at the 80th epoch. In FIGURE 7(a) it can be seen that the sensitivity value in the training process is above 90%. The sensitivity value in the training data and validation data continues to increase. In FIGURE 7(b) it can be seen that the specificity value in the training process for the training data and validation data continues to increase towards a value above 98%. In the 78th epoch the sensitivity and specificity values in the training data and validation data decreased slightly, but increased again and stabilized in the 80th. Dice score and IoU are also measured.

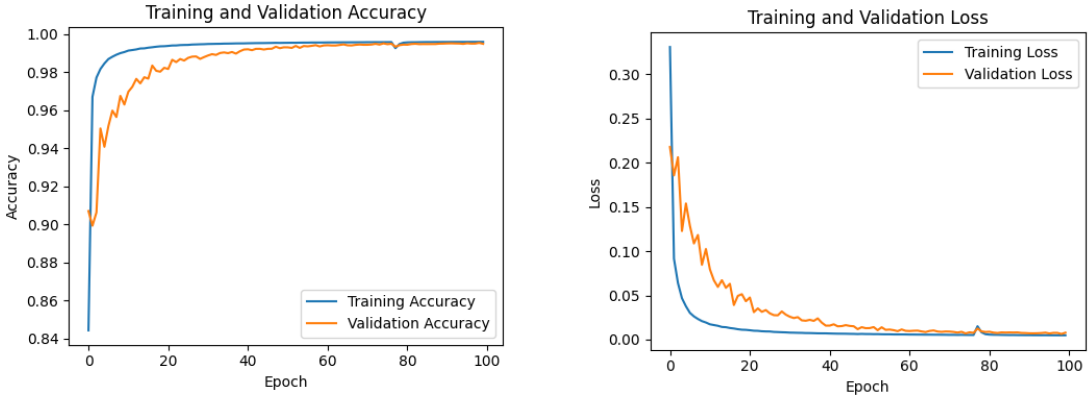

(a) (b)

FIGURE 6. Results of (a) Accuracy and (b) Loss in the Training Process

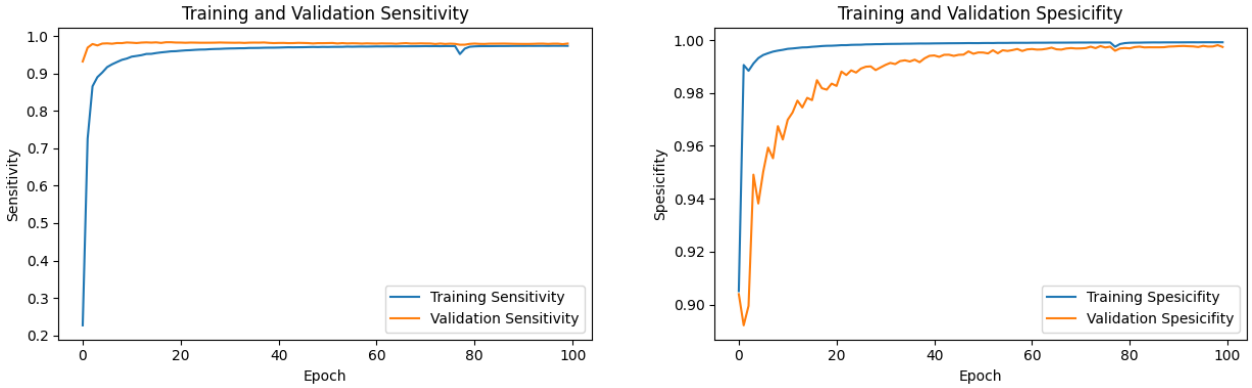

(a) **(b)**

FIGURE 7. Results of (a) Sensitivity and (b) Specificity in the Training Process

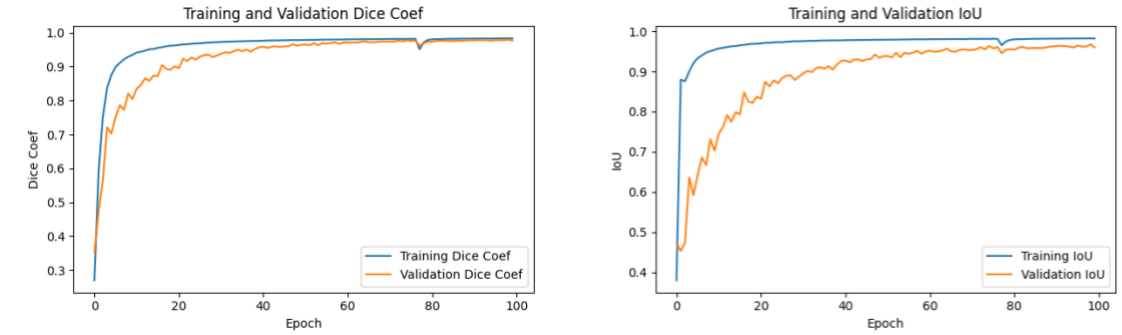

(a) (b)

FIGURE 8. Results of (a) Dice Score and (b) IoU in the Training Process

At the segmentation training stage, dice score and IoU measurements are carried out. The dice score measures the correspondence between the pixels of the segmented image and the pixels of the ground truth image. IoU measures the comparison of the slice area with the combined area between the segmented image and the ground truth image. The graph of the dice score and IoU values in the training process can be seen in FIGURE 8. In FIGURE 8(a), it can be seen that the dice score in the training process is above 90%. The dice score values on the training data and validation data continue to increase from first epoch to last epoch. In FIGURE 8(b), it can be seen that the IoU value in the training process for the training data and validation data continues to increase towards a value above 90%. Based on FIGURE 8, the Dice score and IoU values decreased at epoch 78th. However, at epoch 80th, the values increased stabilized, with both the training and validation data showing an improvement, achieving values above 90% at the end of epoch training stage.

After the training stage, a testing stage was conducted to evaluate the trained model using testing data. This stage involved data that had not been previously processed by the model, specifically testing data used for liver segmentation on CT-Scan images. The testing process applied the best weights from the training stage, representing the model's optimal parameters to ensure accurate performance evaluation. A comparison of the predicted appearance of the liver segmentation results on CT-Scan images with the ground truth can be seen in TABLE 2.

TABLE 2
Comparison of Segmentation and Ground Truth Prediction Results

No	Filename	Original Image	Results	*Ground Truth*
1	Test_ image_2.png	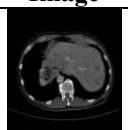		
2	Test_ image_19.png	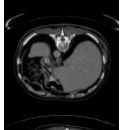	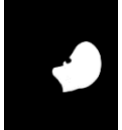	
3	Test_ image_23.png		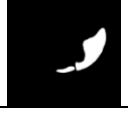	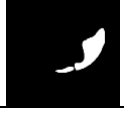

Based on TABLE 2, the results of liver segmentation on CT-scan images are compared for their similarity to the ground truth. Based on the table, it can be seen that the appearance of the predicted image is similar to the appearance of the ground truth image. This shows that the model with the Double U-Net architecture can recognize the liver very well on CT-scan images and is able to segment the liver very well.

C. DISCUSS AND ANALYSIS

This study applies image enhancement methods using CLAHE and a bilateral filter. Image enhancement performance is evaluated using PSNR and SSIM. The PSNR and SSIM values obtained are 40.30 dB and 0.924. To determine the success rate of the contrast enhancement method proposed in this study, the PSNR and SSIM values obtained will be compared with those from other studies that also perform contrast enhancement on CT-scan liver images. A comparison of PSNR and SSIM values with other studies on CT-scan images can be seen in TABLE 3.

TABLE 3
Comparison of PSNR and SSIM Values in CT-Scan Images

No	Image Enhancement Method	PSNR	SSIM
1	Bilateral Filter [44]	35.11	0.56
2	CLAHE [31]	21.46	-
3	Gamma Correction [82]	29.26	0.84
4	Proposed Method	**40.30**	**0.924**

Based on TABLE 3, Nguyen [44] produced good PSNR above 30db, but the SSIM produced was lower than other methods by only applying denoising in the form of bilateral filters without performing contrast enhancement. Siddiqi [31] and Kaur [82] produced PSNR below 30dB by only applying contrast enhancement in the form of CLAHE and Gamma Correction respectively without performing denoising process. The image enhancement method proposed in this study produced the highest PSNR and SSIM values compared to other methods, namely 40.30 and 0.924. The PSNR value indicates that the noise produced by the proposed image enhancement remains at a low level, ensuring minimal distortion. Based on this, the proposed image enhancement method produces very good image quality. The SSIM value shows that the structure of the image enhancement results

using CLAHE and bilateral filters is similar to the original image.

The results of the performance evaluation obtained at the segmentation stage were accuracy and specificity of 99%, sensitivity and Dice score of 98%, and IoU of 97%. The results of the research obtained in this study, were compared with previous studies that had segmented the liver on CT-scan images. Comparisons of the results of liver segmentation on CT-Scan images using the Double U-Net architecture with previous studies can be seen in TABLE 4.

TABLE 4
Comparison of Performance Evaluation Results with Other Research

No.	Method	Acc (%)	Sen (%)	Spe (%)	*DC* (%)	*IoU* (%)
1	Dense-UNet [44]	-	89	-	89	
2	RDC Trans U-Net[83]	98	-	98	93	89
3	MSA U-Net [84]	-	-	98	98	96
4	Marker Controlled Watershed Transform [8]	-	-	-	95	-
5	ANN [85]	98	99	97	-	-
6	Proposed Method	99	98	99	98	97

Based on TABLE 4, the study [44] produced lower sensitivity and dice score than other studies. This study only performed denoising on Liver segmentation using Dense-UNet which produced sensitivity and dice score below 90%. Li et al. [83] produced very good accuracy and specificity. Li et al. [83] only applied grayscale which produced lower IoU than other studies, which was below 90%. Napte et al. [8] produced a high dice score of 95% by applying the Double Gaussian Filter modification to the Marker Controller Watershed Transform, but the resulted dice score was smaller than the MSA U-Net study [84]. Sasirekha et al. [85] produced the highest sensitivity compared to other studies, which was 99% by applying the Gabor Filter to the ANN Method in CT-scan liver segmentation.

Based on TABLE 4, the proposed method has the highest accuracy, specificity, dice score, and IoU values compared to other methods. The proposed method in this study is Double U-Net with the application of a combination of CLAHE and bilateral filters at the image preprocessing stage. The Double U-Net architecture produces a high accuracy of 99%. This shows that the Double U-Net architecture can correctly predict 99% of the pixels in the liver and background features. The results of sensitivity and specificity each show that Double U-Net can correctly predict 98% of the pixels with liver features and 99% of pixels with non-liver features. The sensitivity value obtained in this study was lower than that reported for the ANN model [85]. However, the sensitivity value in this study still reached 98%, indicating that the model is effective in identifying liver features. The result of the dice score shows that 98% of the similarity in the number of pixels overlaps between the ground truth and the segmentation results, while the result of IoU shows that 97% of the total combined area between the segmentation results and the ground truth is in the appropriate overlap. Based on the performance evaluation produced, Double U-Net with the application of a combination of CLAHE and bilateral filters excellent segment the liver on CT-scan liver images.

The results obtained in this study indicate that the proposed model can be utilized in the medical field for the early detection of liver cancer. The utilization of the proposed model in early detection of liver cancer can help medical personnel to perform accurate detection with efficient time. However, for this technology to be implemented in hospitals, cooperation with relevant stakeholders and policy support are required, including regulations for patient data security and training for medical staff. The combination of image enhancement and segmentation methods proposed yields image segmentation results that are similar to the ground truth and demonstrate good performance based on evaluation metrics, but this study is still limited to performing binary segmentation, separating only the liver from the background without considering other important features that may be crucial for early detection of liver cancer. This limitation could be addressed by developing and modifying the proposed method in further research. In future research, the proposed model could be further developed to segment additional features beyond the liver and combined with classification techniques to create a more accurate system for early liver cancer detection.

IV. CONCLUSION

Based on the results of image enhancement using CLAHE and bilateral filter, very good image quality is obtained as indicated by a high PSNR value of above 40dB and SSIM approaching 1. The PSNR value obtained above 40dB indicates that image enhancement using CLAHE and bilateral filter produces very good image quality with little noise intensity. The SSIM resulting from image enhancement with CLAHE and bilateral filter approaching 1 indicates that the enhanced image has a high pixel structure similarity to the original image. The results of liver segmentation on CT-scan images using the Double U-Net architecture produce high performance evaluations. The performance evaluation consisting of accuracy, sensitivity, specificity, dice score, and IoU obtained has a value above 95%. This shows the model can accurately predict each pixel in each feature, and the segmentation results achieve more than 95% overlap with the ground truth, indicating a high degree of similarity between the segmentation output and the ground truth. These findings are valuable in real-world applications, especially in helping doctors analyze CT scan images more quickly and accurately. The next step is to apply this method on other types of medical images and further optimize the model for even better results. For this technology to be widely used, it is important to ensure

that it is accessible to everyone, including those in areas with limited healthcare facilities. This research opens up opportunities for further collaboration between researchers, clinicians, and policymakers to expand the use of AI technology in healthcare.

REFERENCES

[1] X. Li, P. Ramadori, D. Pfister, M. Seehawer, L. Zender, and M. Heikenwalder, "The Immunological and Metabolic Landscape in Primary and Metastatic Liver Cancer," *Nat. Rev. Cancer*, vol. 21, no. 9, pp. 541–557, 2021.

[2] J. Ferlay *et al.*, "Global Cancer Observatory : Cancer Today," *International Journal of Cancer*, 2024.

[3] K. Sridhar, K. C, W.-C. Lai, and B. P. Kavin, "Detection of Liver Tumour Using Deep Learning Based Segmentation with Coot Extreme Learning Model," *Biomedicines*, vol. 11, no. 3, 2023.

[4] J. D. L. Araújo *et al.*, "An automatic method for segmentation of liver lesions in computed tomography images using deep neural networks," *Expert Syst. Appl.*, vol. 180, p. 115064, 2021.

[5] Q. Gu, H. Zhang, R. Cai, S. Y. Sui, and R. Wang, "Segmentation of liver CT images based on weighted medical transformer model," *Sci. Rep.*, vol. 14, no. 1, p. 9887, 2024.

[6] A. M. Anter and A. Ella, "Artificial Intelligence in Medicine CT liver tumor Segmentation Hybrid Approach Using Neutrosophic Sets, Fast Fuzzy C-Means, and Adaptive Watershed Algorithm," *Artif. Intell. Med.*, vol. 97, pp. 1–13, 2019.

[7] A. Mostafa, E. H. Houssein, M. Houseni, A. E. Hassanien, and H. Hefny, "Evaluating Swarm Optimization Algorithms for Segmentation of Liver Images," in *Studies in Computational Intelligence*, vol. 730, 2017, pp. 41–62.

[8] K. M. Napte and A. Mahajan, "Liver Segmentation Using Marker Controlled Watershed Transform," *Int. J. Electr. Comput. Eng.*, vol. 13, no. 2, pp. 1541–1549, 2023, doi: 10.11591/ijece.v13i2.pp1541-1549.

[9] A. V. Vardhan, K. S. Roy, K. Reddy, K. Sainadh, and M. Nannapeni, "Liver Tumor Segmentation using Deep Learning Techniques," *Int. J. Food Nutr. Sci.*, vol. 11, no. 12, pp. 1585–1592, 2023.

[10] D. Mitrea *et al.*, "Liver Tumor Segmentation From Computed Tomography Images Through Convolutional Neural Networks," in *2023 9th International Conference on Systems and Informatics (ICSAI)*, 2023, pp. 1–6.

[11] M. Rahimpour, A. Radwan, H. Vandermeulen, S. Sunaert, K. Goffin, and M. Koole, "Investigating certain choices of CNN configurations for brain lesion segmentation," *arXiv Prepr. arXiv2212.01235*, 2022.

[12] F. Zohourian, J. Siegemund, M. Meuter, and J. Pauli, "Efficient fine-grained road segmentation using superpixel-based CNN and CRF models," *arXiv Prepr. arXiv2207.02844*, 2022.

[13] M. Krithika alias AnbuDevi and K. Suganthi, "Review of Semantic Segmentation of Medical Images Using Modified Architectures of UNET," *Diagnostics*, vol. 12, no. 12. 2022.

[14] N. Siddique, S. Paheding, C. P. Elkin, and V. Devabhaktuni, "U-Net and Its Variants for Medical Image Segmentation: A Review of Theory and Applications," *IEEE Access*, vol. 9, pp. 82031–82057, 2021.

[15] D. U. N. Qomariah, H. Tjandrasa, and C. Fatichah, "Segmentation of Microaneurysms for Early Detection of Diabetic Retinopathy using MResUNet," *Int. J. Intell. Eng. Syst.*, vol. 14, no. 3, pp. 359–373, 2021.

[16] J. Qin, X. Wang, D. Mi, Q. Wu, Z. He, and Y. Tang, "CI-UNet: Application of Segmentation of Medical Images of the Human Torso," *Appl. Sci.*, vol. 13, no. 12, 2023.

[17] H. Lu, Y. She, J. Tie, and S. Xu, "Half-UNet: A Simplified U-Net Architecture for Medical Image Segmentation," *Front. Neuroinform.*, vol. 16, no. June, pp. 1–10, 2022.

[18] C. Li, X. Liu, W. Li, C. Wang, H. Liu, and Y. Yuan, "U-KAN Makes Strong Backbone for Medical Image Segmentation and Generation," *arXiv Prepr. arXiv2406.02918*, 2024.

[19] A. Desiani *et al.*, "Multi-Stage CNN: U-Net and Xcep-Dense of Glaucoma Detection in Retinal Images," *J. Electron. Electromed. Eng. Med. Informatics*, vol. 5, no. 4, pp. 211–222, 2023.

[20] F. Özcan, O. N. Uçan, S. Karaçam, and D. Tunçman, "Fully Automatic Liver and Tumor Segmentation from CT Image Using an AIM-Unet," *Bioengineering*, vol. 10, no. 2, 2023.

[21] Y. A. Ayalew, K. A. Fante, and M. A. Mohammed, "Modified U-Net for liver cancer segmentation from computed tomography images with a new class balancing method.," *BMC Biomed. Eng.*, vol. 3, no. 1, p. 4, Mar. 2021.

[22] Z. Liu *et al.*, "Liver CT sequence segmentation based with improved U-Net and graph cut," *Expert Syst. Appl.*, vol. 126, pp. 54–63, 2019.

[23] Z. Sun, Y. Pang, Y. Sun, and X. Liu, "DMFF-Net: Densely Macroscopic Feature Fusion Network for Fast Magnetic Resonance Image Reconstruction," *Electron.*, vol. 11, no. 23, 2022.

[24] L. Qi *et al.*, "High Quality Entity Segmentation," *Proc. IEEE Int. Conf. Comput. Vis.*, pp. 4024–4033, 2023.

[25] S. U. Saeed *et al.*, "Image quality assessment by overlapping task-specific and task-agnostic measures: application to prostate multiparametric MR images for cancer segmentation," *arXiv Prepr. arXiv2202.09798*, 2022.

[26] S. Almotairi, G. Kareem, M. Aouf, B. Almutairi, and M. A. M. Salem, "Liver tumor segmentation in CT scans using modified segnet," *Sensors (Switzerland)*, vol. 20, no. 5, 2020.

[27] V. Gavini and G. R. J. Lakshmi, "CT Image Denoising Model Using Image Segmentation for Image Quality Enhancement for Liver Tumor Detection Using CNN," *Trait. du Signal*, vol. 39, no. 5, pp. 1807–1814, 2022.

[28] C. T. Jensen *et al.*, "Reduced-Dose Deep Learning Reconstruction for Abdominal CT of Liver Metastases," *Radiology*, vol. 303, no. 1, pp. 90–98, 2022.

[29] R. Naseem, Z. A. Khan, N. Satpute, A. Beghdadi, F. A. Cheikh, and J. Olivares, "Cross-Modality Guided Contrast Enhancement for Improved Liver Tumor Image Segmentation," *IEEE Access*, vol. 9, pp. 118154–118167, 2021.

[30] A. Desiani, M. Erwin, B. Suprihatin, S. Yahdin, A. I. Putri, and F. R. Husein, "Bi-Path Architecture of CNN Segmentation and Classification Method for Cervical Cancer Disorders Based on Pap-smear Images," *Int. J. Comput. Sci.*, vol. 48, no. 3, pp. 1–9, 2021.

[31] A. A. Siddiqi, G. B. Narejo, M. Tariq, and A. Hashmi, "Investigation of Histogram Equalization Filter for CT Scan Image Enhancement," *Biomed. Eng. - Appl. Basis Commun.*, vol. 31, no. 5, pp. 1–10, 2019.

[32] T. P. H. Nguyen, Z. Cai, K. Nguyen, S. Keth, N. Shen, and M. Park, "Pre-processing Image using Brightening, CLAHE and RETINEX," *arXiv Prepr. arXiv2003.10822*, 2020.

[33] M. Hayati *et al.*, "Impact of CLAHE-based image enhancement for diabetic retinopathy classification through deep learning," *Procedia Comput. Sci.*, vol. 216, pp. 57–66, 2023.

[34] D. R. I. M. Setiadi, "PSNR vs SSIM: Imperceptibility Quality Assessment for Image Steganography," *Multimed. Tools Appl.*, vol. 80, no. 6, pp. 8423–8444, 2021.

[35] U. Sara, M. Akter, and M. S. Uddin, "Image Quality Assessment through FSIM, SSIM, MSE and PSNR—A Comparative Study," *J. Comput. Commun.*, vol. 07, no. 03, pp. 8–18, 2019.

[36] A. Gutub and F. Al-Shaarani, "Efficient Implementation of Multi-image Secret Hiding Based on LSB and DWT Steganography Comparisons," *Arab. J. Sci. Eng.*, vol. 45, no. 4, pp. 2631–2644, 2020.

[37] H. H. Liu, P. C. Su, and M. H. Hsu, "An Improved Steganography Method Based on Least-Significant-Bit Substitution and Pixel-Value Differencing," *KSII Trans. Internet Inf. Syst.*, vol. 14, no. 11, pp. 4537–4556, 2020.

[38] A. Desiani *et al.*, "Denoised Non-Local Means with BDDU-Net Architecture for Robust Retinal Blood Vessel Segmentation," *Int. J. Pattern Recognit. Artif. Intell.*, vol. 37, no. 16, pp. 1–27, 2023.

[39] I. Bakurov, M. Buzzelli, R. Schettini, M. Castelli, and L. Vanneschi, "Structural similarity index (SSIM) revisited : A data-driven approach," vol. 189, no. October 2021, 2022.

[40] N. Umilizah, P. Octavia, L. I. Kesuma, I. Rayani, and M. Suedarmin, "Combination of Image Improvement on

Segmentation Using a Convolutional Neural Network in Efforts to Detect Liver Disease," *J. Informatics Telecommun. Eng.*, vol. 7, no. 2, pp. 375–384, 2024.

[41] M. Elhoseny and K. Shankar, "Optimal bilateral filter and Convolutional Neural Network based denoising method of medical image measurements," *Meas. J. Int. Meas. Confed.*, vol. 143, pp. 125–135, 2019.

[42] B. C. Rao, S. S. Rani, K. Shashidhar, G. Satyanarayana, and K. Raju, "An effective image-denoising method with the integration of thresholding and optimized bilateral filtering," *Multimed. Tools Appl.*, vol. 82, no. 28, pp. 43923–43943, 2023.

[43] A. Asokan and J. Anitha, "Adaptive Cuckoo Search based optimal bilateral filtering for denoising of satellite images," *ISA Trans.*, vol. 100, pp. 308–321, 2020.

[44] H. T. Nguyen, M. N. Nguyen, T. Q. Duong, and P. H. D. Bui, "Denoising with Median and Bilateral on CT images for Liver segmentation," in *Proceedings - 2022 RIVF International Conference on Computing and Communication Technologies, RIVF 2022*, 2022, pp. 59–64.

[45] J. Muthuswamy, "New Edge Preserving Hybrid Method for Better Enhancement of Liver CT Images," *Indian J. Sci. Technol.*, vol. 10, no. 10, pp. 1–7, 2017.

[46] J. Kugelman *et al.*, "A comparison of deep learning U-Net architectures for posterior segment OCT retinal layer segmentation," *Sci. Rep.*, vol. 12, no. 1, pp. 1–14, 2022.

[47] D. Jha, M. A. Riegler, D. Johansen, P. Halvorsen, and H. D. Johansen, "DoubleU-Net: A deep convolutional neural network for medical image segmentation," in *Proceedings - IEEE Symposium on Computer-Based Medical Systems*, 2020, vol. 2020-July, no. 1, pp. 558–564.

[48] Y. Liu *et al.*, "Double-branch U-Net for multi-scale organ segmentation," *Methods*, vol. 205, pp. 220–225, 2022.

[49] W. Guo, H. Zhou, Z. Gong, and G. Zhang, "Double U-Nets for Image Segmentation by Integrating the Region and Boundary Information," *IEEE Access*, vol. 9, pp. 69382–69390, 2021.

[50] P. Sangeeta, L. S. Jayanth, K. Chinni, K. J. Chandran, and K. Teja, "Replenishing the Facial Features Behind the Mask Using Unet," *Interantional J. Sci. Res. Eng. Manag.*, vol. 08, no. 06, pp. 1–5, 2024.

[51] Stevenazy, "Liver Dataset," *Kaggle*, 2020.

[52] D. N. A, S. G, D. D. J, and S. P. Kashyap, "Retinopathy Based Multistage Classification of Diabetes," in *Proceedings of the 3rd International Conference on Integrated Intelligent Computing Communication & Security (ICIIC 2021)*, 2021, pp. 54–60.

[53] M. Arhami, Y. R. Fachri, H. Hendrawaty, and A. Adriana, "A Semantic Segmentation of Nucleus and Cytoplasm in Pap-smear Images using Modified U-Net Architecture," *Infotel*, vol. 16, no. 2, pp. 273–288, 2024.

[54] C. Y. Jeong, H. C. Shin, and M. Kim, "Sensor-Data Augmentation for Human Activity Recognition with Time-Warping and Data Masking," *Multimed. Tools Appl.*, vol. 80, no. 14, pp. 20991–21009, 2021.

[55] G. Iglesias, E. Talavera, Á. González-Prieto, A. Mozo, and S. Gómez-Canaval, "Data Augmentation Techniques in Time Series Domain: A Survey and Taxonomy," *Neural Comput. Appl.*, vol. 35, no. 14, pp. 10123–10145, 2023, doi: 10.1007/s00521-023-08459-3.

[56] K. Chaitanya *et al.*, "Semi-Supervised Task-Driven Data Augmentation for Medical Image Segmentation," *Med. Image Anal.*, vol. 68, p. 101934, 2021.

[57] T. Nemoto *et al.*, "Effects of Sample Size and Data Augmentation on U-Net-Based Automatic Segmentation of Various Organs," *Radiol. Phys. Technol.*, vol. 14, no. 3, pp. 318–327, 2021.

[58] N. P. Sutramiani, N. Suciati, and D. Siahaan, "MAT-AGCA: Multi Augmentation Technique on Small Dataset for Balinese Character Recognition using Convolutional Neural Network," *ICT Express*, vol. 7, no. 4, pp. 521–529, 2021.

[59] Y. Jiang, P. Malliaras, B. Chen, and D. Kulić, "Model-Based Data Augmentation for User-Independent Fatigue Estimation," *Comput. Biol. Med.*, vol. 137, no. September, pp. 1–11, 2021.

[60] K. Maharana, S. Mondal, and B. Nemade, "A Review: Data Pre-processing and Data Augmentation Techniques," *Glob. Transitions Proc.*, vol. 3, no. 1, pp. 91–99, 2022.

[61] C. Bhardwaj, S. Jain, and M. Sood, "Diabetic Retinopathy Severity Grading Employing Quadrant-Based Inception-V3 Convolution Neural Network Architecture," *Int. J. Imaging Syst. Technol.*, vol. 31, no. 2, pp. 592–608, 2021.

[62] T. Kumar, R. Brennan, A. Mileo, and M. Bendechache, "Image Data Augmentation Approaches : A Comprehensive Survey and Future Directions," *IEEE Access*, vol. 4, pp. 1–36, 2024.

[63] A. Desiani, D. A. Zayanti, R. Primartha, F. Efriliyanti, and N. A. C. Andriani, "Variasi Thresholding untuk Segmentasi Pembuluh Darah Citra Retina," *J. Edukasi dan Penelit. Inform.*, vol. 7, no. 2, p. 255, 2021.

[64] B. Kim, R. O. Serfa Juan, D. E. Lee, and Z. Chen, "Importance of Image Enhancement and CDF for Fault Assessment of Photovoltaic Module using IR Thermal Image," *Appl. Sci.*, vol. 11, no. 18, 2021.

[65] J. Dash and N. Bhoi, "Retinal Blood Vessel Segmentation using Otsu Thresholding with Principal Component Analysis," *Proc. 2nd Int. Conf. Inven. Syst. Control. ICISC 2018*, no. Icisc, pp. 933–937, 2018.

[66] S. Singh, N. Mittal, and H. Singh, "Multifocus Image Fusion Based on Multiresolution Pyramid and Bilateral Filter," *IETE J. Res.*, vol. 68, no. 4, pp. 2476–2487, 2022.

[67] A. B. A., A. P. P., and V. Maik, "Contrast and Luminance Enhancement Technique for Fundus Images Using Bi-Orthogonal Wavelet Transform and Bilateral Filter," *ECS J. Solid State Sci. Technol.*, vol. 10, no. 7, p. 071010, 2021.

[68] P. Naveen and P. Sivakumar, "Adaptive Morphological and Bilateral Filtering with Ensemble Convolutional Neural Network for Pose-Invariant Face Recognition," *J. Ambient Intell. Humaniz. Comput.*, vol. 12, no. 11, pp. 10023–10033, 2021.

[69] T. Guo, J. Dong, H. Li, and Y. Gao, "Simple Convolutional Neural Network on Image Classification," in *International Conference on Big Data Analysis*, 2017, pp. 721–724.

[70] C. P. Parmo, L. I. Kesuma, and D. Geovani, "The Combination of Black Hat Transform and U-Net in Image Enhancement and Blood Vessel Segmentation in Retinal Images," *Comput. Eng. Appl.*, vol. 12, no. 3, pp. 129–145, 2023.

[71] S. Ioffe and C. Szegedy, "Batch Normalization: Accelerating Deep Network Training by Reducing Internal Covariate Shift," *Journal. Pract.*, vol. 10, no. 6, pp. 730–743, 2016.

[72] S. Ngah and R. A. Bakar, "Sigmoid Function Implementation using The Unequal Segmentation of Differential Lookup Table and Second Order Nonlinear Function," *Telecommun. Electron. Comput. Eng.*, vol. 9, no. 2–8, pp. 103–108, 2017.

[73] A. Panja, J. J. Christy, and Q. M. Abdul, "An Approach to Skin Cancer Detection using Keras and Tensorflow," *J. Phys. Conf. Ser.*, vol. 1911, no. 1, pp. 1–8, 2021.

[74] U. Ruby, P. Theerthagiri, J. Jacob, and V. Vamsidhar, "Binary Cross Entropy with Deep Learning Technique for Image Classification," *Int. J. Adv. Trends Comput. Sci. Eng.*, vol. 9, no. 4, pp. 5393–5397, 2020.

[75] R. Yu, Y. Wang, Z. Zou, and L. Wang, "Convolutional Neural Networks with Refined Loss Functions for The Real-time Crash Risk Analysis," *Transp. Res. Part C Emerg. Technol.*, vol. 119, no. April, p. 102740, 2020.

[76] J. H. J. C. Ortega, A. C. Lagman, L. R. Q. Natividad, E. T. Bantug, M. R. Resureccion, and L. O. Manalo, "Analysis of Performance of Classification Algorithms in Mushroom Poisonous Detection using Confusion Matrix Analysis," *Int. J. Adv. Trends Comput. Sci. Eng.*, vol. 9, no. 1.3, pp. 451–456, 2020.

[77] N. Maleki, Y. Zeinali, and S. T. A. Niaki, "A K-NN Method for Lung Cancer Prognosis with The Use of A Genetic Algorithm for Feature Selection," *Expert Syst. Appl.*, vol. 164, no. July 2019, p. 113981, 2021.

[78] S. K. Hou, Z. G. Ou, P. X. Qin, Y. L. Wang, and Y. R. Liu, "Image-based Crack Recognition of Tunnel Lining using Residual U-Net Convolutional Neural Network," *IOP Conf. Ser. Earth Environ. Sci.*, vol. 861, no. 7, pp. 1–11, 202.

[79] S. M. González-collazo *et al.*, "Santiago Urban Dataset SUD : Combination of Handled and Mobile Laser Scanning point clouds," 2020.

[80] J. Huang *et al.*, "DBFU-Net: Double Branch Fusion U- Net with Hard Example Weighting Train Strategy to Segment Retinal

Vessel," *PeerJ Comput. Sci.*, vol. 8, pp. 1–29, 2022.
[81] F. Rahmad, Y. Suryanto, and K. Ramli, "Performance Comparison of Anti-Spam Technology Using Confusion Matrix Classification," in *IOP Conference Series: Materials Science and Engineering*, 2020, vol. 879, no. 1.
[82] H. Kaur, N. Kaur, and N. Neeru, "A Comparative Study of Image Enhancement Algorithms for Abdomen CT Images," *2024 IEEE Int. Conf. Interdiscip. Approaches Technol. Manag. Soc. Innov. IATMSI 2024*, vol. 2, pp. 1–6, 2024.
[83] L. Li and H. Ma, "RDCTrans U-Net: A Hybrid Variable Architecture for Liver CT Image Segmentation," *Sensors*, vol. 22, no. 7. 2022.
[84] J. Wu *et al.*, "U-Net combined with multi-scale attention mechanism for liver segmentation in CT images," *BMC Med. Inform. Decis. Mak.*, vol. 21, no. 1, pp. 1–12, 2021.
[85] N. Sasirekha, R. Anitha, V. T, and U. Balakrishnan, "Automatic liver tumor segmentation from CT images using random forest algorithm," *Sci. Temper*, vol. 14, no. 03, pp. 696–702, 2023.

Dwi Fitri Brianna https://orcid.org/0009-0000-9848-5867 was born in Palembang, Indonesia, in 1996. Graduated from the Informatics Engineering Study Program, Faculty of Computer Science, Bina Darma University in 2017 as the best graduate. Graduated from the Informatics Engineering Masters Study Program, Bina Darma University in 2019 as the best graduate. Currently a permanent lecturer in the Informatics Department, Faculty of Computer Science, Sjakhyakirti University, Palembang.

Lucky Indra Kesuma https://orcid.org/0000-0002-8112-4659 was born in Palembang on September 25, 1990. He completed his education as an Associate Degree in Computerized Accounting in 2011 at Sriwijaya University. He continued his education for a Bachelor's degree in Information Systems, graduating in 2014 from Sriwijaya University. He then pursued a Master's degree in Computer Science, specializing in Informatics Engineering, completing his studies in 2017 at Bina Darma University. In 2023, he finished his doctoral studies (Ph.D.) in Engineering Science (Informatics). The author is a permanent lecturer in the Information Systems program at the Faculty of Computer Science, Sjakhyakirti University, Palembang, and is actively engaged in the Tri Dharma (Three Pillars of Higher Education).

Dite Geovani https://orcid.org/0009-0000-8377-8683 was born in Palembang, Januari 2002. She is currently working on a project for Doctoral Program at Engineering Faculty, Universitas Sriwijaya. She received a bachelor's degree in Mathematics from Universitas Sriwijaya in 2023 and is currently undergoing a PMDSU scholarship program at Universitas Sriwijaya since 2023. Her current research includes the fields of image processing, pattern recognition, data mining, and artificial intelligence.

Puspa Sari https://orcid.org/0009-0006-1738-6087 was born in Lubuk Linggau, Februari 2002. She currently working on a project for his undergraduate degree at Mathematics Department, science and Nature Faculty, Universitas Sriwijaya. In 2024, She joined the Laboratory of Computation Mathematics and Natural Science Faculty, Universitas Sriwijaya as an Assistant Lecturer. Her current research includes the field of image processing, pattern recognition and computer vision, data mining,and artificial intelligence.